X-Ray Structural and Photoluminescence Spectroscopic Investigation of the Europium Octamolybdate Polymer $Eu_2(H_2O)_{12}[Mo_8O_{27}]\cdot 6H_2O$ and Intramolecular Energy Transfer in the Crystalline Lattice†

Toshihiro Yamase* and Haruo Naruke

Research Laboratory of Resources Utilization, Tokyo Institute of Technology, 4259 Nagatsuta, Midori-ku, Yokohama 227, Japan

Photoluminescence and intramolecular energy-transfer properties of $Eu_2(H_2O)_{12}[Mo_8O_{27}]\cdot 6H_2O$, **1** have been determined in connection with the crystal structure. The compound has been prepared by treating $K_2[MoO_4]$ with $Eu(NO_3)_3$ in aqueous solution at pH 3.0 and isolated in a crystalline form with a belt structure. A single-crystal X-ray analysis [triclinic, space group $P\bar{1}$, a = 10.105(3), b = 12.006(5), c = 9.365(4) Å, α = 122.59(3), β = 90.12(3), γ = 98.33(3)°, Z = 1, Mo-Kα radiation, R = 0.063 for 4485 independent data with $I > 3\sigma(I)$] shows the cation to have the composition $[Eu(H_2O)_6]^{3+}$. The latter is also bonded to one oxygen atom of each octahedron of an edge-sharing pair of MoO_6 octahedra in the Mo_8O_{27} anion, which is isostructural to the condensation polymer of the octamolybdate through one common oxygen atom. In addition, Eu^{3+} is linked by one oxygen atom belonging to the MoO_6 octahedron in a neighbouring Mo_7O_{27} unit, resulting in the formation of a tricapped trigonal-prismatic $Eu(H_2O)_6O_3$ group (average Eu–O bond length 2.48 Å). Luminescent transitions of both $^5D_0 \longrightarrow {}^7F_J$ and $^5D_1 \longrightarrow {}^7F_J$ for Eu^{3+} are observed upon photoexcitation of the O→Mo ligand-to-metal charge-transfer (l.m.c.t.) bands but the intramolecular energy transfer to the $^5D_1$ level takes place predominantly from the O→Mo l.m.c.t. states at energies higher than 3.6 eV (*ca.* 5.8×10^{-19} J). The temperature dependence of the intramolecular energy transfer from the O→Mo l.m.c.t. states to Eu^{3+} indicates that the configuration of the Mo–O–Eu linkage (*ca.* 150°) allows hopping of a d^1 electron to the EuO_9 site due to thermally activated delocalization between MoO_6 and EuO_9 sites, which acts as a deactivation channel for the energy transfer from the O→Mo l.m.c.t. states to the emitting levels of Eu^{3+}. Co-ordination of six aqua ligands leads to a low lifetime (0.17 ± 0.01 ms) of the emitting state of $^5D_0$ with a resultant decrease in the total quantum yields of the emission, arising from vibronic coupling of the $^5D_0$ state with the vibrational states of high-frequency OH oscillators. The $^7F_1$, $^7F_2$, $^7F_3$, $^7F_4$, $^5D_1$ and $^5D_2$ crystal-field splittings for the C_1 site of Eu^{3+} are estimated on the basis of the high-resolution emission and excitation spectra at 77 K. Vibronic lines belonging to the $^7F_0 \longrightarrow {}^5D_2$ and $^7F_1 \longrightarrow {}^6D_1$ transitions are observed in the excitation spectrum.

Photoexcitation of the oxygen-to-metal charge transfer (O→M l.m.c.t.) band of polyoxometalates is followed by a recombination between the electron and hole. When several energy levels exist in the O→M l.m.c.t. bands, energy transfer occurs from the O→M l.m.c.t. excited states to these levels, as demonstrated for polyoxotungstoeuropates: energy transfer from the O→W l.m.c.t. excited states to Eu^{3+} in polyoxotungstoeuropate lattices has been studied using $K_{15}H_3[Eu_3(H_2O)_3(SbW_9O_{33})(W_5O_{18})_3]\cdot 25.5H_2O$, $Na_9[Eu(W_5O_{18})_2]\cdot 18H_2O$ and $K_{13}[Eu(SiW_{11}O_{39})_2]\cdot 3H_2O$.[1–4] All of the Eu^{3+} ions in these three complexes prepared in aqueous solutions show eight-co-ordination by oxygen atoms. A comparison of both the lifetime ($\tau_{c.t.}$) and total quantum yield ($\varphi_{c.t.}$) of the emission from the $^5D_0$ level upon photoexcitation of the O→W l.m.c.t. bands of the complexes indicates that the hopping of a d^1 electron between WO_6 octahedra is the predominant deactivation channel of the O→W l.m.c.t. levels, which induces a decrease in the rate of the energy transfer to the $^5D_0$ state of Eu^{3+}.[1] The direct co-ordination of aqua ligands to Eu^{3+} results in small values of $\tau_{c.t.}$ and $\varphi_{c.t.}$, probably due to a weak coupling of the $^5D_0$ state with the vibrational states of the high-frequency OH oscillators.[1,5] The number (n) of water molecules co-ordinated to Eu^{3+} has been estimated experimentally, with an uncertainty of 0.5, from equation (1) where k_{H_2O} and k_{D_2O} are the reciprocals (in ms^{-1}) of the experimental lifetimes in a water or D_2O environment.[6] Using the lifetimes obtained for water and D_2O solutions, thus, it has been reported that $[Eu(W_5O_{18})_2]^{9-}$ has four water molecules co-ordinated to Eu^{3+} in dilute aqueous solutions and that n decreases with increasing concentration of $[Eu(W_5O_{18})_2]^{9-}$, to zero in the solid state.[3] Although X-ray crystallography would enable us to characterize the structure of the first co-ordination sphere of Eu^{3+}, the only polyoxometaloeuropates of known crystal structure are $K_{15}H_3[Eu_3(H_2O)_3(SbW_9O_{33})(W_5O_{18})_3]\cdot 25.5H_2O$ and $[NH_4]_{12}H_2[Eu_4(H_2O)_{16}(MoO_4)(Mo_7O_{24})_4]\cdot 13H_2O$.[1,5] Each Eu^{3+} in the former was found to be co-ordinated to two H_2O, SbW_9O_{33} and W_5O_{18} ligands forming an eight-co-ordination by oxygen atoms, in the latter to four H_2O, two Mo_7O_{24} and one MoO_4 ligands forming a nine-co-ordinate, distorted, tricapped trigonal prism.

$$n = 1.05(k_{H_2O} - k_{D_2O}) \quad (1)$$

To understand the effects of polyoxometalate and aqua ligands on the energy transfer in the polyoxometaloeuropate lattices, we have recently characterized europium octamolybdate polymer, $Eu_2(H_2O)_{12}[Mo_8O_{27}]\cdot 6H_2O$, **1**.[5] In the present study, we focus on this system, for which X-ray crystallographic and photoluminescence measurements have helped us to en-

† *Supplementary data available:* see Instructions for Authors, *J. Chem. Soc., Dalton Trans.*, 1991, Issue 1, pp. xviii–xxii.

large the knowledge of the intramolecular energy transfer in polyoxometalate lattices. Also of interest is the description of the crystal-field splittings of the ^7F and ^5D Russell–Saunders terms on the basis of the high-resolution spectra for both $^5D_0 \longrightarrow {}^7F_J$ and $^5D_1 \longrightarrow {}^7F_J$ emissions.

Experimental

Preparation and Chemical Analysis.—All the reagents required for the preparation were used without further purifications. The compound $Eu_2(H_2O)_{12}[Mo_8O_{27}]\cdot 6H_2O$, **1**, was prepared by the following method. The salt $K_2[MoO_4]$ (3.2 g) was dissolved in water (1200 cm^3) and the solution acidified by $HClO_4$ to pH 3. Then, $Eu(NO_3)_3\cdot 6H_2O$ (3.8 g) in water (50 cm^3) was added dropwise with stirring and the mixture was kept at room temperature. Within 7 d pale yellow crystals of **1** were precipitated.

Molybdenum was determined by the KSCN–$SnCl_2$ method (colorimetry at 475 nm).[7] Europium was determined by back titration with $MnSO_4$ in the presence of 0.01 mol dm^{-3} ethylenediaminetetraacetate, NH_3–NH_4Cl buffer of pH 10, and Eriochrom Black T indicator.[8] Thermogravimetric analysis (Rigaku, Thermoflex TG-DGC) was used for the determination of water of crystallization {Found: Eu, 16.8; Mo, 40.2; H_2O, 13.2. Calc. for $Eu_2(H_2O)_{12}[Mo_8O_{27}]\cdot 6H_2O$ ($H_{36}Eu_2Mo_8O_{45}$): Eu, 16.6; Mo, 42.0; H_2O, 17.7%}. Other polyoxomolybdolanthanates containing La, Ce, Pr, Nd, Sm, Tb and Dy were synthesized by a similar procedure. The compounds $K_{15}H_3[Eu_3(H_2O)_3(SbW_9O_{33})(W_5O_{18})_3]\cdot 25.5H_2O$, **2**,[1] $[NH_4]_{12}H_2[Eu_4(H_2O)_{16}(MoO_4)(Mo_7O_{24})_4]\cdot 13H_2O$, **3**,[5] $[NH_3Pr^i]_6[Mo_8O_{26}(OH)_2]\cdot 2H_2O$[9] and $[NH_4]_6[Mo_8O_{27}]\cdot 4H_2O$[10] were prepared as described previously.

X-Ray Crystallography.—Accurate unit-cell parameters were determined by least-squares treatment of the angular coordinates of 18 reflections with $2\theta = 20$–$30°$ measured with a Rigaku four-circle RASA-5II diffractometer.

Crystal data. $Eu_2Mo_8O_{27}\cdot 18H_2O$ **1**, $M = 1827.7$, triclinic, space group $P\bar{1}$, $a = 10.105(3)$, $b = 12.006(5)$, $c = 9.365(4)$ Å, $\alpha = 122.59(3)$, $\beta = 90.12(3)$, $\gamma = 98.33(3)°$, $U = 942.8(7)$ Å^3, $D_m = 3.166$ g cm^{-3} (pycnometrically), $Z = 1$, $D_c = 3.219$ g cm^{-3}, $F(000) = 677.6$, and μ(Mo-Kα) = 55.14 cm^{-1}.

A crystal with approximate dimensions 0.40 × 0.05 × 0.01 mm was mounted on the tip of a glass fibre in air. Intensities were collected in the range $2 < 2\theta < 60°$ using graphite-monochromatized Mo-Kα ($\lambda = 0.710\,68$ Å) radiation and the ω–2θ scan technique at a 2θ scan rate of 8° min^{-1}. Lorentz and polarization factors were applied and an absorption correction was made using the program DABEX.[11] Correction factors were from 1.028 to 1.140. Of 5991 independent reflections, 4485 having $I > 3\sigma(I)$, were retained for the refinement of the structure. The positions of Mo and Eu atoms were obtained by a direct method using MULTAN 78.[12] The atomic scattering factors and anomalous dispersion terms were taken from ref. 13. Calculations were carried out on the HITAC 660 K computer at this Institute. The structure was refined using the SHELX 76 package of programs.[14] The quantity minimized was $\Sigma w(|F_o| - |F_c|)^2$. The refinement converged to R(unweighted) = 0.063 and $R' = 0.109$ $\{w = 1.5305[\sigma^2(F_o) + 0.0116\ F_o^2]^{-1}\}$ for 195 parameters. No extinction coefficient was applied. The maximum and minimum heights in the final difference synthesis were 3.2 and −2.6 e Å^{-3} respectively, around a water oxygen atom at a distance of 0.65 Å in the region of the solvent.

Additional material available from the Cambridge Crystallographic Data Centre comprises thermal parameters and remaining bond lengths and angles.

Spectral Measurements.—Sample powders were prepared by grinding single crystals of compound **1** in an agate mortar. Diffuse reflectance and IR spectra at 300 K were recorded on Hitachi 330 and JASCO IRA-2 spectrophotometers, respectively. The reflectance spectrum at 77 K was obtained as follows: light from a 500 W xenon lamp was passed through a chopper and monochromator (Nikon G-25 grating monochromator) and was split into reference and sample beams by a beam splitter (1 : 1). The sample beam was then focused on the sample pellet (thickness about 0.5 mm) placed on a brass plate inside a liquid-nitrogen Dewar with a quartz window of optical quality and reflected into the photomultiplier (Hamamatsu TV R636) tube at an angle of 60° with respect to the irradiation beam, after passing through a filter (Toshiba V-44) for elimination of the emission wavelengths. A ratiometer was used to divide output from the photomultiplier tube by output from the reference beam, when recording the spectrum so as to correct for changes in signal intensity due to wavelength-dependent variations in the output of the monitoring light and in the sensitivity of the monochromator/photomultiplier tube arrangement. The modulated part of the signal was analysed using a lock-in amplifier (NF L1-574). The reference channel of the amplifier was driven by a photocell positioned so as to detect the reference beam. The total spectral range was covered by a wavelength scan from 460 to 370 nm.

Emission and excitation spectra were obtained according to the method described previously.[1] The time profiles of the luminescence from both the $^5D_0$ and $^5D_1$ states of Eu^{3+} under excitation with a pulsed NRG 0.9 – 5 – 90 nitrogen laser (337 nm) were obtained with a Tektronix 2230 digital storage oscilloscope. The emission quantum yields were evaluated by the method of Haas and Stein[15] using $Na_9[Eu(W_5O_{18})_2]\cdot 18H_2O$ ($\varphi = 0.80$) as a standard for 310 nm excitation.[2,3] High-resolution emission spectra were obtained on a JASCO CT-1000 D double monochromator using the nitrogen laser for excitation. High-resolution excitation spectra were obtained with a Molectron DL-14P dye (coumarin 460, LD 473, coumarin 500, coumarin 540A, disodium fluorescein and rhodamine 590) laser pumped by a Molectron UV-24 nitrogen laser. The high-resolution spectra were recorded with a slit width resolution of 1 cm^{-1} and an absolute frequency accuracy of ± 1 cm^{-1} is estimated on the basis of the dye-laser alignment.

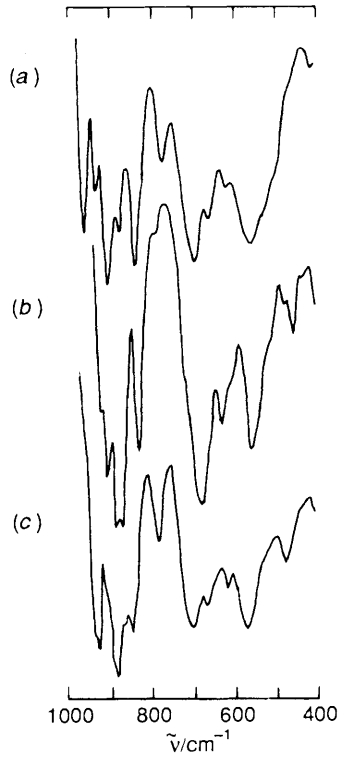

Fig. 1 IR spectra of compound **1** (*a*), $[NH_3Pr^i]_6[Mo_8O_{26}(OH)_2]\cdot 2H_2O$ (*b*), and $[NH_4]_6[Mo_8O_{27}]\cdot 4H_2O$ (*c*)

Table 1 Atomic coordinates ($\times 10^4$ for Mo and Eu, $\times 10^3$ for oxygen) for $Eu_2(H_2O)_{12}[Mo_8O_{27}]\cdot 6H_2O$ with estimated standard deviations (e.s.d.s) in parentheses

Atom	*x*	*y*	*z*	Atom	*x*	*y*	*z*
Eu(1)	8104(1)	2225(1)	8383(1)	Mo(1)	5536(1)	2625(1)	1916(1)
Mo(2)	4188(1)	4114(1)	5839(1)	Mo(3)	7522(1)	3614(1)	5263(1)
Mo(4)	3448(1)	4643(1)	897(1)				
O(1)	807(1)	268(1)	600(1)	O(2)	383(1)	554(1)	555(1)
O(3)	475(1)	402(1)	202(1)	O(4)	635(1)	210(1)	323(1)
O(5)	500	500	0	O(6)	775(1)	529(1)	732(1)
O(7)	688(1)	268(1)	80(1)	O(8)	558(1)	361(1)	658(1)
O(9)	445(1)	122(1)	45(1)	O(10)	722(1)	696(1)	64(1)
O(11)	751(1)	438(1)	935(1)	O(12)	387(1)	276(1)	371(1)
O(13)	285(1)	390(1)	677(1)	O(14)	881(1)	386(1)	426(1)
$O_w(1)$	159(1)	973(1)	437(1)	$O_w(2)$	948(1)	399(1)	131(1)
$O_w(3)$	582(1)	163(1)	706(1)	$O_w(4)$	29(1)	326(1)	808(1)
$O_w(5)$	693(1)	13(1)	812(2)	$O_w(6)$	670(1)	969(1)	295(1)
$O_w(7)$	15(2)	880(2)	120(2)	$O_w(8)$	36(2)	146(2)	402(2)
$O_w(9)$	135(2)	202(2)	167(2)				

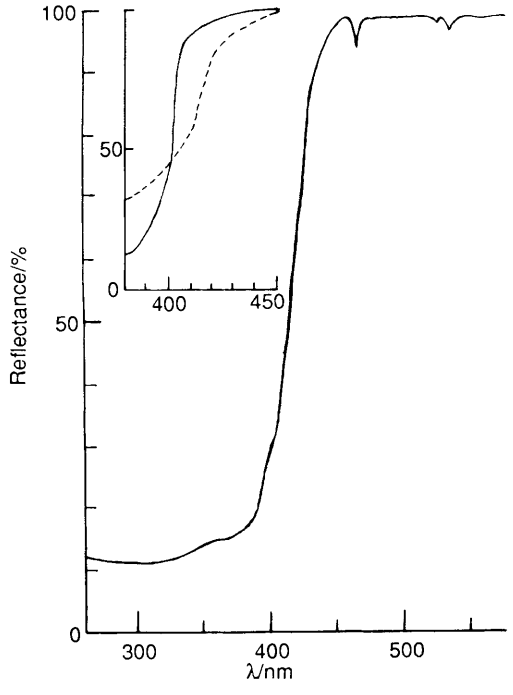

Fig. 2 Diffuse reflectance spectrum of compound **1** at 300 K. Inset: reflectance spectra at 77 (——) and 300 (– – –) K when other conditions are kept constant.

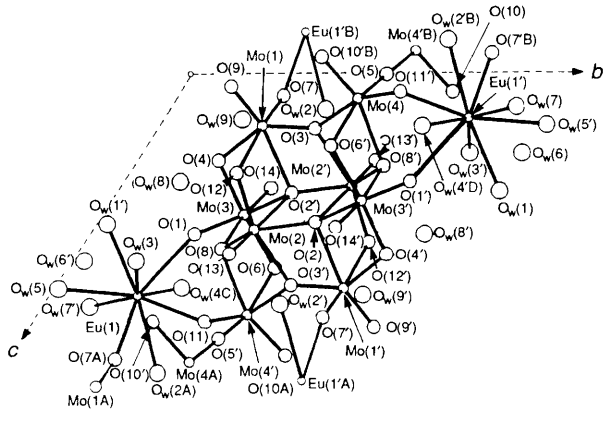

Fig. 3 Structure of compound **1** viewed along the *a* axis. Primed atoms are related to the corresponding unprimed ones by an inversion centre. The notation A–D denotes atoms in the adjacent unit having symmetry codes (*x*, *y*, 1 + *z*), (*x*, *y*, −1 + *z*), (1 + *x*, *y*, *z*) and (−*x*, 1 − *y*, 1 − *z*) respectively.

Results

IR and Electronic Spectra.—Fig. 1 shows the 400–1000 cm^{-1} regions of the IR spectra of three complexes with the octamolybdate unit, $Eu_2(H_2O)_{12}[Mo_8O_{27}]\cdot 6H_2O$, **1**, $[NH_3Pr^i]_6[Mo_8O_{26}(OH)_2]\cdot 2H_2O$ and $[NH_4]_6[Mo_8O_{27}]\cdot 4H_2O$. All the spectra are similar at 500–1000 cm^{-1}, suggesting that an octamolybdate unit is common to the three complexes. The symmetric and asymmetric stretchings of the different kinds of Mo–O bonds are observed at 960–580 cm^{-1}: probably Mo=O (960–880 cm^{-1}), Mo–O–Mo corner-sharing bridge (860–840 cm^{-1}), Mo–OH (870 cm^{-1}) and Mo–O–Mo edge-sharing bridge (790–680 cm^{-1}).[16,18] Fig. 2 shows the diffuse reflectance spectrum of powdered compound **1** at 300 K. The feature of the spectrum is the presence of intense broad bands with the absorption edge at about 440 nm in the UV wavelength region due to the O→Mo l.m.c.t. transitions. The O→Eu l.m.c.t. bands are expected to lie in the region 240–250 nm but they have small absorption coefficients and thus they are obscured by the intense polyoxomolybdate bands.[3] There are three weak lines due to the f–f transitions: $^7F_1 \longrightarrow {}^5D_1$ (at about 535 nm), $^7F_0 \longrightarrow {}^5D_1$ (about 525 nm) and $^7F_0 \longrightarrow {}^5D_2$ (about 465 nm). The band of the $^7F_0 \longrightarrow {}^5L_6$ transition at about 395 nm, which was observed for the polyoxotungstoeuropates,[1] is buried in the strong absorption of the O→Mo l.m.c.t. transition.

Crystallographic Characterization of $Eu_2(H_2O)_{12}[Mo_8O_{27}]\cdot 6H_2O$, **1**.—The final positional parameters of compound **1** are given in Table 1, selected bond lengths and angles in Table 2 and distances between the heavy atoms in Table 3. Fig. 3 shows the structure of the octamolybdate unit in a projection parallel to the *a* axis. The units are connected through one common oxygen O(5) atom on a special position, forming the condensation polymer of the octamolybdate $\{[Mo_8O_{27}]^{6-}\}_\infty$ which is isostructural to the anion of $[NH_4]_6[Mo_8O_{27}]\cdot 4H_2O$.[10] Additional binding to Eu(1) [or Eu(1′)] through O(1) [or O(1′)], O(7A) [or O(7′B)] and O(11) [or O(11′)] atoms should be noted and results in formation of an infinite belt of the octamolybdate running parallel to the *c* axis, as shown in Fig. 4. The belt structure of **1** is the reason for the lack of solubility in water. The Mo–O bond lengths for the octamolybdate unit vary from 1.68(1) to 2.50(1) Å, with values of 1.68(1)–1.70(1) Å for the terminal Mo=O bonds. The Mo···Mo distances range from 3.246(2) [Mo(1)···Mo(3)] to 3.505(2) Å [Mo(2)···Mo(2′)] for edge-sharing MoO_6 octahedra and 3.767(2) [Mo(4)···Mo(4′B)] to 3.985(2) Å [Mo(2)···Mo(3′)] for the corner-sharing octahedra. The shortest Mo···Mo distance [3.767(2) Å] for the corner-sharing octahedra involves different octameric units through two-co-ordinated atom O(5), while 3.899(2) and 3.985(2) Å are for the octahedra within the octameric units through three- and four-co-ordinate atoms O(3) and O(2)

Table 2 Selected bond lengths (Å) and angles (°) for $Eu_2(H_2O)_{12}$-$[Mo_8O_{27}]\cdot 6H_2O$ with e.s.d.s in parentheses

Eu(1)–O(1)	2.58(1)	Eu(1)–O_w(3)	2.44(1)
Eu(1)–O(7)	2.41(1^{I})	Eu(1)–O_w(4)	2.47(1^{III})
Eu(1)–O(11)	2.41(1)	Eu(1)–O_w(5)	2.51(2)
Eu(1)–O_w(1)	2.44(1^{II})	Eu(1)–O_w(7)	2.43(2^{II})
Eu(1)–O_w(2)	2.61(1^{I})		
Mo(1)–O(2)	2.20(1^{II})	Mo(2)–O(2)	1.95(1)
Mo(1)–O(3)	1.91(1)	Mo(2)–O(2)	2.50(1^{II})
Mo(1)–O(4)	1.89(1)	Mo(2)–O(3)	2.16(1^{II})
Mo(1)–O(7)	1.74(1)	Mo(2)–O(8)	1.87(1)
Mo(1)–O(9)	1.70(1)	Mo(2)–O(12)	1.76(1)
Mo(1)–O(12)	2.34(1)	Mo(2)–O(13)	1.68(1)
Mo(3)–O(1)	1.74(1)	Mo(4)–O(3)	2.13(1)
Mo(3)–O(2)	2.17(1^{II})	Mo(4)–O(5)	1.88(1)
Mo(3)–O(4)	2.00(1)	Mo(4)–O(6)	2.04(1^{II})
Mo(3)–O(6)	1.87(1)	Mo(4)–O(8)	2.24(1^{II})
Mo(3)–O(8)	2.32(1)	Mo(4)–O(10)	1.70(1^{II})
Mo(3)–O(14)	1.69(1)	Mo(4)–O(11)	1.73(1^{II})
O(1)–Eu(1)–O_w(2A)	120.0(4)	Mo(1)–O(3)–Mo(2′)	106.5(6)
O(1)–Eu(1)–O_w(5)	124.7(5)	Mo(1)–O(3)–Mo(4)	149.7(7)
O(11)–Eu(1)–O_w(5)	134.3(5)	Mo(1)–O(4)–Mo(3)	113.2(6)
O(11)–Eu(1)–O_w(3)	77.3(4)	Mo(1)–O(12)–Mo(2)	116.1(6)
O(11)–Eu(1)–O_w(4C)	83.3(4)	Mo(1)–O(2′)–Mo(2)	95.8(4)
O(11)–Eu(1)–O(7A)	76.8(4)	Mo(1)–O(2′)–Mo(3)	95.9(4)
O_w(5)–Eu(1)–O_w(2A)	115.3(5)	Mo(1)–O(2′)–Mo(2′)	103.3(5)
O_w(5)–Eu(1)–O_w(4C)	142.2(5)	Mo(2)–O(8)–Mo(3)	112.8(5)
O_w(3)–Eu(1)–O_w(1′)	81.8(5)	Mo(2)–O(2′)–Mo(2′)	103.2(5)
O_w(3)–Eu(1)–O(7A)	80.5(4)	Mo(2)–O(3′)–Mo(4′)	103.3(5)
O_w(7′)–Eu(1)–O(7A)	99.4(6)	Mo(3)–O(2′)–Mo(2′)	150.4(6)
O_w(7′)–Eu(1)–O_w(4C)	71.8(6)	Mo(3)–O(6)–Mo(4′)	114.2(6)
Eu(1)–O(1)–Mo(3)	147.3(6)	Mo(4)–O(8′)–Mo(2′)	109.6(5)
Eu(1)–O(11)–Mo(4′)	150.5(7)	Mo(4)–O(8′)–Mo(3′)	92.1(4)
Eu(1)–O(7A)–Mo(1A)	158.4(7)	Mo(4)–O(5)–Mo(4′B)	179.9(1)

Symmetry equivalent positions: I $x, y, 1 + z$; II $1 - x, 1 - y, 1 - z$; III $1 + x, y, z$.

Table 3 Distances (Å) between heavy atoms

Eu(1)···Mo(3)	4.146(2)	Eu(1)···Mo(1A)	4.074(2)
Eu(1)···Mo(4′)	4.005(2)		
Mo(1)···Mo(4)	3.899(2)	Mo(2)···Mo(3)	3.500(2)
Mo(1)···Mo(2)	3.493(2)	Mo(2)···Mo(2′)	3.505(2)
Mo(1)···Mo(3)	3.246(2)	Mo(2)···Mo(3′)	3.985(2)
Mo(1)···Mo(2′)	3.262(2)	Mo(2)···Mo(1′)	3.262(2)
Mo(4)···Mo(3′)	3.283(2)	Mo(2)···Mo(4′)	3.362(2)
Mo(4)···Mo(4′B)	3.767(2)		

respectively. The connection of the belt polymers in the *a* and *b* directions is *via* hydrogen bonds among oxygen atoms of the octameric units and crystal water oxygen (O_w) atoms, as shown in Fig. 4, where O···O_w and O_w···O_w distances within the hydrogen bridges vary from 2.70(2) [O(8)···O_w(3)] to 3.30(2) Å [O_w(1′)···O_w(4C)]. Many of the hydrogen bonds occur as bifurcated bridges.

Fig. 5 shows the environment of the Eu atom in compound **1**. Atom Eu(1) is nine-co-ordinate with the positions of the oxygen atoms approximating a tricapped trigonal prism. The average Eu–O distance is 2.48 Å. The atoms O(1), O_w(5) and O_w(2A) (with an average Eu–O bond length of 2.57 Å) approximately cap the faces of the prism and are at a greater distance from Eu(1) than six other oxygen atoms (with an average Eu–O bond length of 2.43 Å), O(7A), O(11), O_w(1′), O_w(3), O_w(4C) and O_w(7′), which are situated at the vertices of the trigonal prism. The three bond angles subtended at the europium site by the Eu-capped oxygen bonds are 124.7(5), 120.0(4) and 115.3(5)°, which sum to 360°, implying a planar arrangement for the Eu and the three capped oxygen atoms. All four atoms lie nearly in

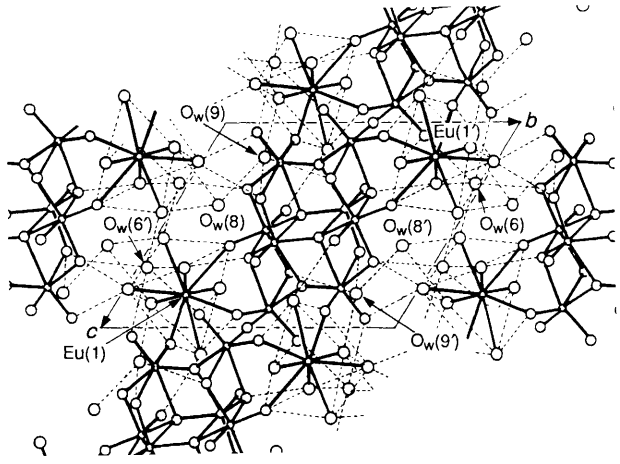

Fig. 4 Condensed polymer of compound **1** and plausible hydrogen-bonding scheme

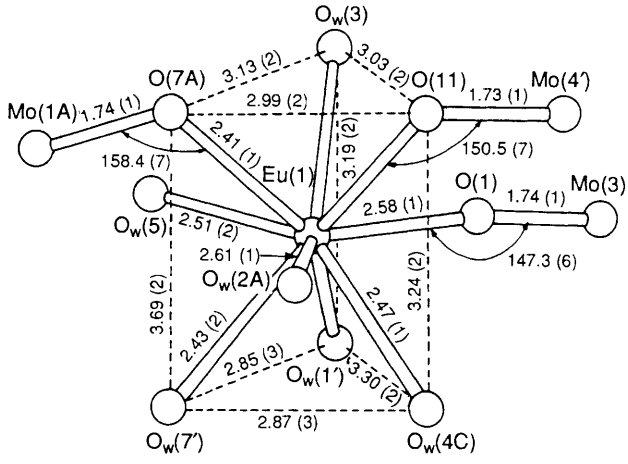

Fig. 5 Distorted tricapped trigonal-prismatic Eu(1) centre with selected interatomic distances (Å) and angles (°)

the same plane except for a small deviation by the Eu, which lies 0.02 Å distant from the horizontal plane. The Eu atom also lies slightly out of each plane including a capped atom and the two atoms of an opposite edge at the europium site. The idealized symmetry of a tricapped trigonal prism is D_{3h}, but since all the ligating atoms of the europium site are not identical the highest possible symmetry about the Eu atom would be C_2. In addition, since the sterically induced geometrical distortions at each MoO_6 octahedron in the octamolybdate are included, the symmetry about the europium centre is reduced to C_1.

Photoluminescence Properties.—Photoexcitation of the O→Mo l.m.c.t. bands of compound **1** gives the emission of Eu^{3+}. Fig. 6 shows the low- and high-resolution emission spectra at 77 K for excitation with 337 nm light. The emission originates from both $^5D_0$ and $^5D_1$ excited states of Eu^{3+}. The luminescent transitions all terminate in the $J = 0$–4 levels of the ground ^7F_J state. However, the weak $^5D_1 \longrightarrow {}^7F_4$ transition, which will appear at about 613.7, 616.9 and 620.0 nm, is superimposed in the region of the strong $^5D_0 \longrightarrow {}^7F_2$ transition. The identification of all emitting levels associated with Eu^{3+} is made on the basis of the luminescence data.[6,19] Every $^5D_1 \longrightarrow {}^7F_J$ emission is very weak in intensity and its total yield is about 3% of the $^5D_0 \longrightarrow {}^7F_J$ emission at 77 K. The relative intensities of the $^5D_0 \longrightarrow {}^7F_2$ and $^5D_1 \longrightarrow {}^7F_1$ emissions are the highest of the $^5D_0 \longrightarrow {}^7F_J$ and $^5D_1 \longrightarrow {}^7F_J$ emissions, respectively. The intensity ratio of the $^5D_{0,1} \longrightarrow {}^7F_J$ lines was little dependent on the temperature in the range 300–4.2 K. A single sharp $^5D_0 \longrightarrow {}^7F_0$ line is observed at 579.42(2) nm, thus placing the

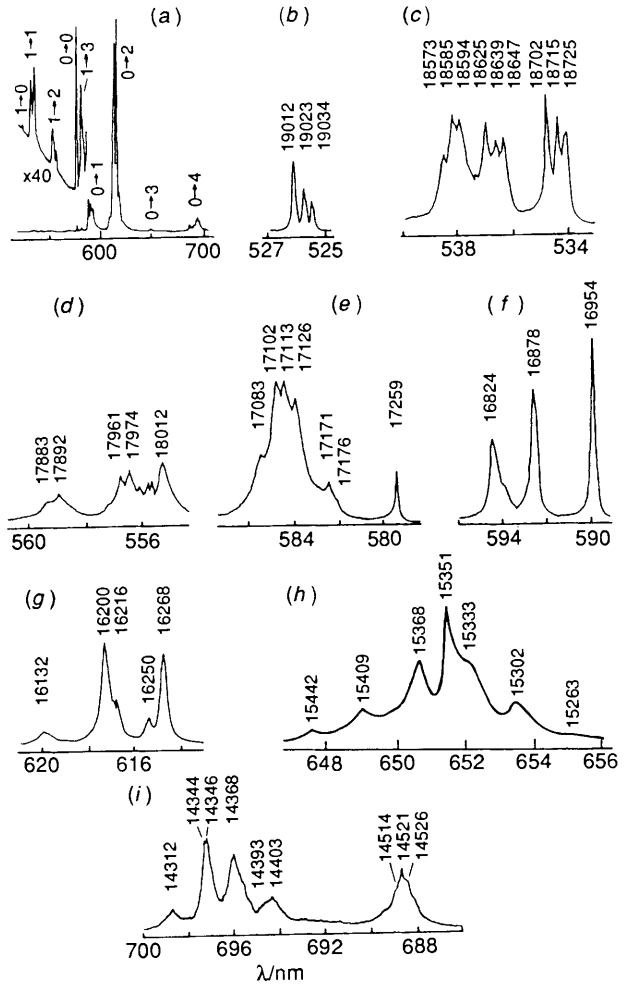

Fig. 6 Emission spectra of compound **1** at 77 K under low (*a*) and high [(*b*)–(*i*)] resolution. Numbers in (*a*) indicate $J \longrightarrow J'$ for the $^5D_J \longrightarrow {}^7F_{J'}$ transitions. The positions of the emission lines in (*b*)–(*i*) are indicated in frequency units. All of the transition energies in (*d*) are not necessarily indicated for clarity.

energy of the $^5D_0$ state at 17 259(1) cm^{-1}.* A triplet of $^5D_1 \longrightarrow {}^7F_0$ lines at 77 K occurs at 525.98(2), 525.67(2) and 525.39(2) nm and these lines identify three levels ($^5D_{1a}$, $^5D_{1b}$ and $^5D_{1c}$) of the $^5D_1$ excited state at 19 012(1), 19 023(1) and 19 034(1) cm^{-1}. Since the $^5D_0 \longrightarrow {}^7F_0$ transition cannot be split by any crystal field, the above observations indicate the presence of a single distinct emitting Eu^{3+} centre that resides in a low-symmetry environment. Correlations of the number of observed luminescence peaks with the number predicted on the basis of symmetry considerations allow us to determine the molecular point group of this centre.[20,21] A comparison of the selection rules governing the $^5D_0 \longrightarrow {}^7F_J$ emissive transitions with the present work implies that Eu^{3+} occupies a site of C_1 symmetry, as shown crystallographically (Fig. 5).

The low-resolution excitation spectra recorded with the $^5D_0 \longrightarrow {}^7F_2$ and $^5D_1 \longrightarrow {}^7F_1$ analysing wavelengths at 300, 77 and 4.2 K are shown in Figs. 7 and 8 respectively, where the spectrum at $\lambda < 440$ nm is corrected for the wavelength dependence of the excitation path and then normalized. The spectrum consists of broad bands due to the O→Mo l.m.c.t. absorption and a large number of lines due to the transition within the $4f^6$ configuration of Eu^{3+}, including the $^7F_0 \longrightarrow {}^5L_6$ transition at 395 nm. Normalized excitation spectra indicate that the O→Mo l.m.c.t. bands consist of four components, A (290 nm), B (340 nm), C (370 nm) and D (410 nm). The excitation into the low-

* The standard errors given in parentheses refer to the last decimal place given.

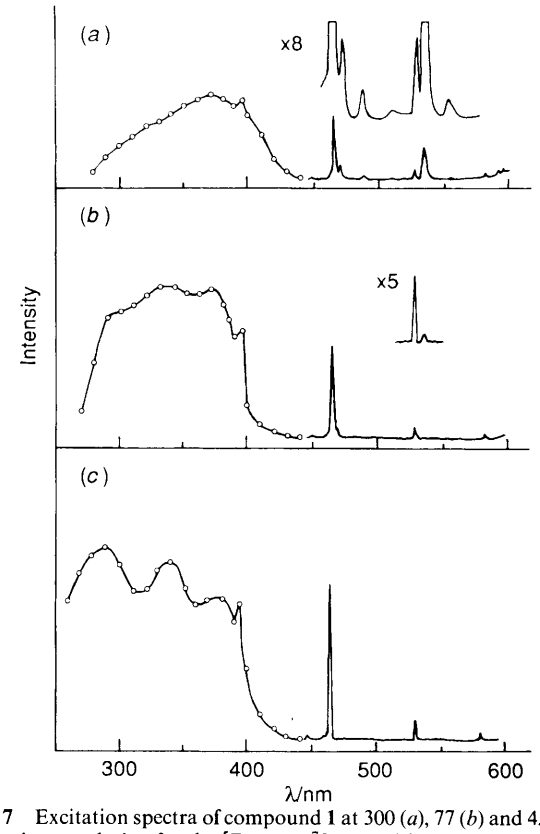

Fig. 7 Excitation spectra of compound **1** at 300 (*a*), 77 (*b*) and 4.2 K (*c*) under low resolution for the $^5D_0 \longrightarrow {}^7F_2$ transition (615 nm)

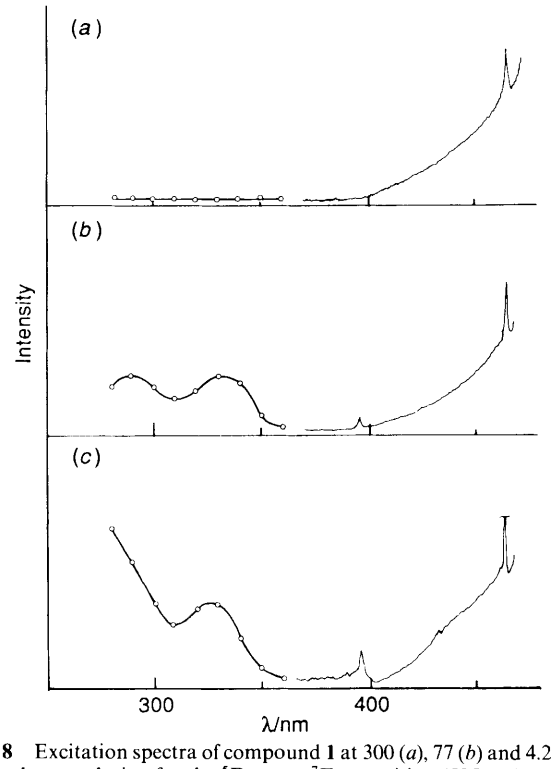

Fig. 8 Excitation spectra of compound **1** at 300 (*a*), 77 (*b*) and 4.2 K (*c*) under low resolution for the $^5D_1 \longrightarrow {}^7F_1$ transition (535 nm)

lying O→Mo l.m.c.t. states, bands C and D, skips the $^5D_1$ level during their relaxation process. The temperature dependence of the normalized excitation spectra indicates that the distribution of the bands A–C increases with decreasing temperature, while one of the D bands decreases at low temperature. This may be associated with the phenomenon that in strongly absorbing crystals excitation into the absorption maximum is not very effective because it cannot enter the crystal and considerable radiationless losses occur in the surface layer,[2] as suggested

Table 4 The $^5D_0$ and $^5D_1$ emission decay ($\tau_{c.t.}$) and total emission quantum yield upon excitation of the O→Mo l.m.c.t. bands of compound **1**

	$^5D_0 \longrightarrow {}^7F_J$						$^5D_1 \longrightarrow {}^7F_J$					
	$10^4\tau_{c.t.}$/s			$\varphi_{c.t.}$			$10^6\tau_{c.t.}$/s			$\varphi_{c.t.}$		
Excitation light wavelength/nm	300	77	4.2 K	300	77	4.2 K	300	77	4.2 K	300	77	4.2 K
290	—	—	—	0.005 (0.07)*	0.023 (0.14)*	0.036 (—)*	—	—	—	—	—	3×10^{-3}
337	1.7 ± 0.1 (2.0 ± 0.1)*	1.7 ± 0.1 (2.4 ± 0.1)*	1.6 (—)*	—	—	—	5 (5)*	12 ± 1 (11 ± 1)*	13 (—)*	—	—	—
340	—	—	—	0.013 (0.07)*	0.029 (0.12)*	0.034 (—)*	—	—	—	—	1×10^{-3}	1×10^{-3}
370	—	—	—	0.016	0.028	0.027	—	—	—	—	≈0	≈0

* $\tau_{c.t.}$ and $\varphi_{c.t.}$ values for compound **3** presented for comparison. The measurement at 4.2 K for **3** was difficult because of its degradation.

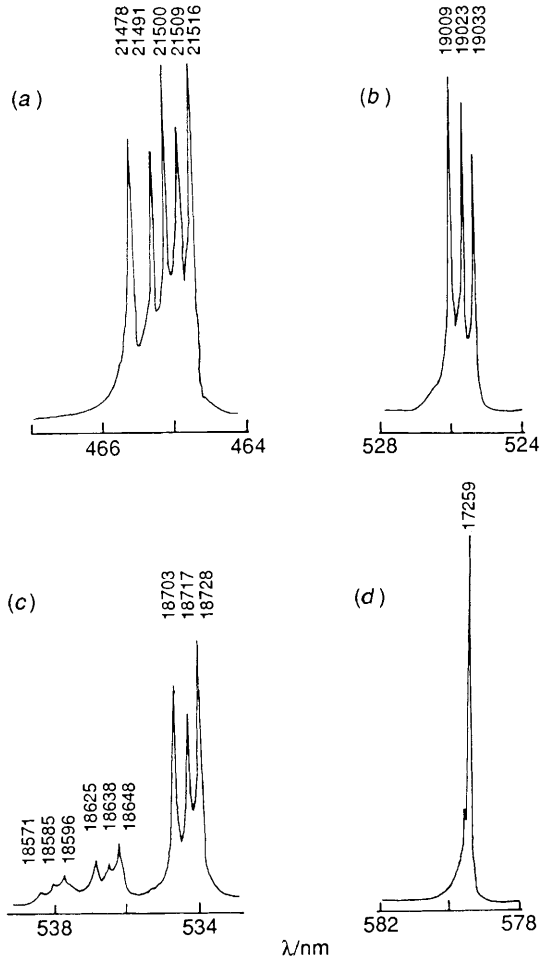

Fig. 9 High-resolution excitation spectra of compound **1** at 77 K for the $^5D_0 \longrightarrow {}^7F_2$ transition (615 nm): (*a*)–(*d*) indicate $^7F_0 \longrightarrow {}^5D_2$, $^7F_0 \longrightarrow {}^5D_1$, $^7F_1 \longrightarrow {}^5D_1$ and $^7F_0 \longrightarrow {}^5D_0$ spectra, respectively

by a difference in the composition of the reflectance spectra at 77 and 300 K (inset in Fig. 2). Furthermore, a decrease in the temperature induces a reduction in the intensities of the transitions from $^7F_1$ states at about 473 ($^7F_1 \longrightarrow {}^5D_2$), 535 ($^7F_1 \longrightarrow {}^5D_1$) and 591 nm ($^7F_1 \longrightarrow {}^5D_0$) owing to the Boltzmann factor intensity dependence.[1] Several lines at about 488, 511 and 555 nm, which are assigned to vibronic lines belonging to the $^7F_0 \longrightarrow {}^5D_2$ (for the first two) and $^7F_1 \longrightarrow {}^5D_1$ (for the latter) transitions as discussed below, disappear at temperatures ≤77 K. The excitation into the $^7F_0 \longrightarrow {}^5D_2$ band yields stronger $^5D_1 \longrightarrow {}^7F_J$ emission than into any wavelengths of the A or B bands. High-resolution excitation spectra of the $^5D_0 \longrightarrow {}^7F_2$ emission at 77 K in the $^7F_0 \longrightarrow {}^5D_{0,1,2}$ and $^7F_1 \longrightarrow {}^5D_1$ regions are shown in Fig. 9. The high-resolution $^7F_0 \longrightarrow {}^5D_1$ spectrum at 77 K is comprised of three main components labelled by a–c. Each is in good agreement with the corresponding $^5D_1 \longrightarrow {}^7F_0$ component of the emission spectrum (Fig. 6). The $^7F_0 \longrightarrow {}^5D_2$ spectrum displays five lines by Stark splitting into $2J + 1$ states, correlating with the C_1 symmetry of the Eu^{3+} site. Evacuation of the glass capillary containing the sample powder caused partial expulsion of the crystal water molecule from the lattice, creating at least three different sites for the emitting Eu^{3+} centre, as indicated by both splitting of the $^5D_0 \longrightarrow {}^7F_0$ line into at least three components and additional complicated $^5D_{0,1} \longrightarrow {}^7F_J$ lines in the emission spectrum.

Measurement of emission decay curves with the 337 nm excitation gave exponential decays for both the $^5D_0 \longrightarrow {}^7F_J$ and $^5D_1 \longrightarrow {}^7F_J$ transitions. Table 4 summarizes the lifetimes ($\tau_{c.t.}$) and the quantum yields ($\varphi_{c.t.}$) with the O→Mo l.m.c.t. excitation at 300, 77 and 4.2 K. The $\tau_{c.t.}$[$(1.7 \pm 0.1) \times 10^{-4}$ s] for the $^5D_0 \longrightarrow {}^7F_J$ transition is almost independent of temperature in the range 300–4.2 K, while $\tau_{c.t.}$[$(5–13) \times 10^{-6}$ s] for the $^5D_1 \longrightarrow {}^7F_J$ transition increases with decreasing temperature.

Discussion

Intramolecular Energy Transfer.—The intramolecular energy transfer from the O→W l.m.c.t. excited state of the polyoxotungstate ligands to the emitting $^5D_0$ level of Eu^{3+} is strongly affected by the configuration of the WO_6 octahedra of the ligands:[1] ligands consisting of edge-sharing WO_6 octahedra with W–O–W bond angles of about 100° result in high values of $\varphi_{c.t.}$ and a small dependence of $\varphi_{c.t.}$ on the temperature, while ligands involved in the corner-sharing WO_6 octahedra with W–O–W bond angles of about 150° *via* a two-co-ordinate oxygen atom exhibit a strong dependence of $\varphi_{c.t.}$ on the temperature. This has been explained by the thermally activated hopping of a d^1 electron between the corner-sharing WO_6 octahedra upon photoexcitation into the O→W l.m.c.t. bands,[1,22–25] which is followed by the deactivated recombination between the electron and hole. Thus, it is anticipated that a large degree of the localization of the d^1 electron at a single MO_6 octahedron in the O→M l.m.c.t. excited states for the polyoxometalate ligand will provide high $\varphi_{c.t.}$ and little dependence of $\varphi_{c.t.}$ on the temperature, as exemplified by $Na_9[Eu(W_5O_{18})_2]\cdot 18H_2O$.[2,3] The configuration of the condensed MoO_6 octahedra in compound **1** shows that the octahedron of Mo(4) is corner-shared with that of Mo(4′B) of the neighbouring anion *via* two-co-ordinate atom O(5) and a nearly linear conformation [Mo(4)–O(5)–Mo(4′B) 179.9(1)° and Mo(4)–O(5) 1.883(1) Å] and that other octahedra of the Mo(1–3) sites are edge-sharing (Fig. 3). Since most parts (about 3/4 = 75%) of the photoexcitation into the O→Mo l.m.c.t. bands of **1** take place at the edge-sharing MoO_6 octahedra, therefore, a small dependence of $\varphi_{c.t.}$ on the

temperature may be expected. However, $\varphi_{c.t.}$ is significantly dependent on the temperature (Table 4 and Figs. 7 and 8). Similar results were observed for $[NH_4]_{12}H_2[Eu_4(H_2O)_{16}(MoO_4)(Mo_7O_{24})_4]\cdot 13H_2O$, **3**, containing edge-shared MoO_6 octahedral Mo_7O_{24} ligands with Mo–O–Mo bond angles of 87–118°,[5] as shown for comparison in Table 4. Thus, another channel for the deactivation of the O→Mo l.m.c.t. excited states can be suggested to elucidate the significant effect of the temperature on $\varphi_{c.t.}$. The degree of delocalization of the d^1 electron in the polyoxometaloeuropate lattices must also be influenced by the conformation of the M–O–Eu linkage in addition to the M–O–M bonding in the ligand. The bond angles Mo–O–Eu at the Eu(1) centre (Fig. 5) are about 150°, Mo(3)–O(1)–Eu(1) 147.3(6), Mo(4′)–O(11)–Eu(1) 150.5(7) and Mo(1A)–O(7A)–Eu(1) 158.4(7)°. Therefore, it is reasonable to assume that photoexcitation into the O→Mo l.m.c.t. bands at the Mo(3), Mo(4′) and Mo(1A) sites allows hopping of the d^1 electron to the $Eu(1)O_9$ site *via* two-co-ordinate oxygen 2p orbitals, since d_π–p_π–f_π orbital mixing for the Mo–O–Eu linkage between the MoO_6 and EuO_9 sites would occur with a mode similar to the d_π–p_π–d_π orbital mixing of the corner-sharing WO_6 octahedra with W–O–W bond angles of 142–155°.[22–27] Then, the decrease in the distribution of the O→Mo l.m.c.t. (A to C) bands with increasing temperature in the excitation spectra for both the $^5D_0 \longrightarrow {}^7F_J$ and $^5D_1 \longrightarrow {}^7F_J$ emissions can be explained in terms of thermally activated hopping of the d^1 electron among the MoO_6 and EuO_9 sites. The Mo–O–Eu bond angles for compound **3** are in the range 147–157°.[5] Therefore, the similar dependence of $\varphi_{c.t.}$ on the temperature for **3** supports the conclusion that the hopping of the d^1 electron between the M–O–Eu linkage is an additional thermal deactivation channel for the intramolecular energy transfer. The deactivation channel of the intramolecular energy transfer at the M–O–Eu linkage with the bond angle of about 150° is operative for the polyoxotungstoeruopates, too. The W–O–Eu bond angles for $[Eu(W_5O_{18})_2]^{9-}$ are in the range 128–132°, since the anion of $Na_9[Eu(W_5O_{18})_2]\cdot 18H_2O$ would be isostructural to that of $Na_6H_2[Ce(W_5O_{18})_2]\cdot 30H_2O$ (space group $C2/c$, $Z = 4$, $U = 6214$ Å^3) even if their sodium salts were not isomorphous because of different crystal packing.[28] The compound $K_{15}H_3[Eu_3(H_2O)_3(SbW_9O_{33})(W_5O_{18})_3]\cdot 25.5H_2O$, **2**, exhibiting a moderate decrease in $\varphi_{c.t.}$ with increasing temperature, indicates two types of W–O–Eu bond angles: 122–127 and 149–153° for the linkage of Eu with W_5O_{18} and SbW_9O_{33} moieties, respectively.[1] Thus, the difference in the temperature effect on $\varphi_{c.t.}$ between $Na_9[Eu(W_5O_{18})_2]\cdot 18H_2O$ and **2** supports the conclusion that thermally activated delocalization of the d^1 electron among the WO_6 and EuO_8 sites, leading to a temperature dependence of $\varphi_{c.t.}$, is unlikely for W–O–Eu bond angles of about 130° {for $Na_9[Eu(W_5O_{18})_2]\cdot 18H_2O$} but operative for W–O–Eu bond angles of about 150° (for the linkage of EuO_8 with the SbW_9O_{33} moiety in **2**). The orbital mixing reflected by the delocalization of the d^1 electron seems to enhance the probability of internal deactivation of the recombination between the d^1 electron and hole in the relaxation of the O→M l.m.c.t. excited state, leading to a decrease in the probability of energy transfer to Eu^{3+} in the lattice.

The excitation spectrum for the $^5D_0 \longrightarrow {}^7F_2$ emission shows a decrease in the distribution of the D band with a decrease in temperature (Fig. 7). This feature may be ascribed to a decrease in the absorption strength of the D band with decreasing temperature, as the reflectance spectrum of compound **1** exhibited a decrease in absorbance at around the D band at 77 K where a reliable interpretation was not allowed (inset in Fig. 2).

Luminescence Spectroscopy.—The $\varphi_{c.t.} = (2.3–2.9) \times 10^{-2}$ for the $^5D_0 \longrightarrow {}^7F_J$ emission of compound **1** at 77 K is nearly one fifth of that (0.12–0.14) for **3** containing four aqua ligands ($n = 4$) at each Eu^{3+} site (Table 4). Since the Eu^{3+} centre of **1** possesses $n = 6$ (Fig. 5), the lower value of $\varphi_{c.t.}$ can be associated with radiationless deactivation of the $^5D_0$ state by the aqua ligands, resulting from the weak vibronic coupling with the vibrational states of the high-frequency OH oscillators.[3,6] As shown in Table 4, the $^5D_0 \longrightarrow {}^7F_J$ emission indicates that $\tau_{c.t.}$ for **1** is lower than for **3**, while the $^5D_1 \longrightarrow {}^7F_J$ emission exhibits no significant difference in $\tau_{c.t.}$ between the two complexes. This supports strongly the deactivation of the $^5D_0$ state by the aqua ligands. The $\tau_{c.t.}$ for the $^5D_0 \longrightarrow {}^7F_J$ emission is little dependent on the temperature but $\tau_{c.t.}$ for the $^5D_1 \longrightarrow {}^7F_J$ emission increases with decreasing temperature. The difference in the temperature effect on $\tau_{c.t.}$ between the two emissions implies that the rate of the non-radiative deactivation from $^5D_1$ to $^5D_0$ levels increases with increasing temperature. From values of $\tau_{c.t.}$ and $\varphi_{c.t.}$ at 4.2 K, where the intramolecular energy transfer from the O→Mo l.m.c.t. excited states to Eu^{3+} will occur efficiently, the radiative transition rates from the $^5D_0$ and $^5D_1$ levels for compound **1** can be estimated to be 2×10^2 and 8×10^1 s^{-1} ($= \varphi_{c.t.}/\tau_{c.t.}$), respectively.

Energies of the $^5D_0 \longrightarrow {}^7F_0$ (single line), $^5D_1 \longrightarrow {}^7F_0$ (three levels) and $^5D_1 \longrightarrow {}^7F_1$ (nine levels) transitions in the high-resolution emission spectrum at 77 K are in good agreement with corresponding energies of the $^7F_0 \longrightarrow {}^5D_0$, $^7F_0 \longrightarrow {}^5D_1$ and $^7F_1 \longrightarrow {}^5D_1$ transitions in the high-resolution excitation spectrum at 77 K, within experimental errors (Figs. 6 and 9). This enabled us to calculate each energy level of the crystal-field components of both $^5D_1$ and $^7F_1$ states. Furthermore, high-resolution $^5D_0 \longrightarrow {}^7F_2$ emission and $^7F_0 \longrightarrow {}^5D_2$ excitation spectra (five lines for each) let us determine each genuine crystal-field component of the $^7F_2$ and $^5D_2$ states, respectively. Similarly, each component of the $^7F_3$

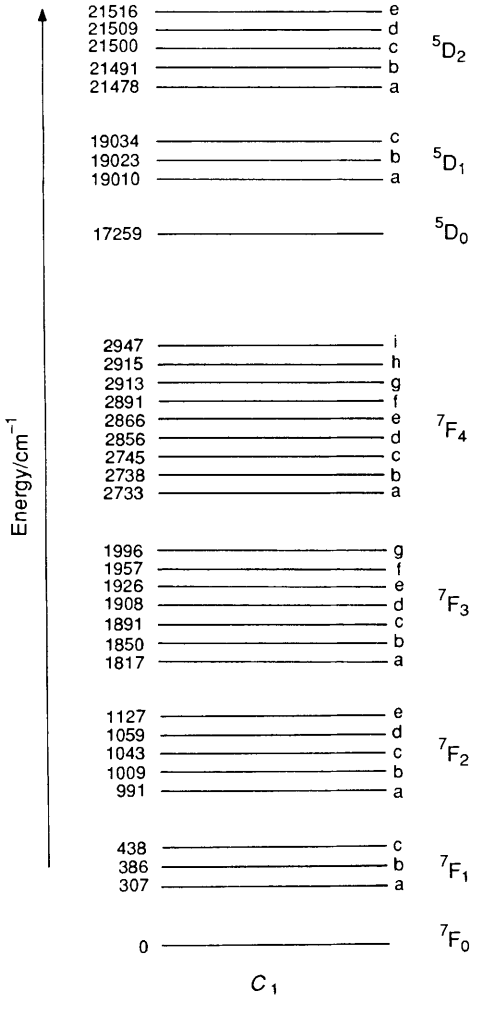

Fig. 10 Energy-level diagram of the Eu^{3+} site in compound **1**. Values are calculated with an accuracy of ± 2 cm^{-1}.

(seven levels) and $^7F_4$ (nine levels) states can be estimated from the high-resolution $^5D_0 \longrightarrow {}^7F_3$ and $^5D_0 \longrightarrow {}^7F_4$ emission spectrum at 77 K, respectively (Fig. 6). The results for the energy-level scheme are shown in Fig. 10.

The excitation spectrum of the $^5D_0 \longrightarrow {}^7F_2$ emission at 300 K (Fig. 7) contains several broad lines at 487.5, 511.2 and 555.5 nm, where the high-resolution spectra exhibit unresolved broad bands. The first two and the latter lines are located at lower energies than the intense $^7F_0 \longrightarrow {}^5D_2$ and $^7F_1 \longrightarrow {}^5D_1$ transitions, respectively. The energy differences between the $^7F_0 \longrightarrow {}^5D_{2a}$ line (21 478 cm^{-1}) and the lines at 487.5 and 511.2 nm are 965 and 1916 cm^{-1}, respectively. These values correspond to the Mo=O stretching vibration at about 960 cm^{-1} (Fig. 1) and its second harmonics, respectively, within the accuracy. Similarly, the energy difference between the line at 555.5 nm and the $^7F_{1a} \longrightarrow {}^5D_{1a}$ line (18 703 cm^{-1}) is 701 cm^{-1} which corresponds to the Mo–O stretching vibration (700 cm^{-1}) for the edge-sharing Mo–O–Mo bridge (Fig. 1). Other components for the $^7F_0 \longrightarrow {}^5D_2$, $^7F_1 \longrightarrow {}^5D_2$ or $^7F_{0,1} \longrightarrow {}^5D_1$ transitions hardly match with the two Mo–O stretching vibrations. Since the above three lines are broad and weak and greatly temperature-dependent, therefore, the lines at 487.5 and 511.2 nm and that at 555.5 nm can be assigned to vibronic lines belonging to the strong $^7F_0 \longrightarrow {}^5D_{2a}$ and $^7F_{1a} \longrightarrow {}^5D_{1a}$ transitions, respectively.[29,30] The line at 511.2 nm is much weaker than that at 487.5 nm, supporting the conclusion that the former is due to coupling with the second harmonics of the Mo=O vibration. It is interesting that each of the Mo=O and Mo–O–Mo vibrational modes is coupled with a different ^7F state, $^7F_0$ and $^7F_{1a}$, respectively.

Acknowledgements

We are indebted to Professor T. Hirose and Mr. N. Akamatsu for providing facilities for high-resolution emission and excitation spectral measurements.

References

1 T. Yamase, H. Naruke and Y. Sasaki, *J. Chem. Soc., Dalton Trans.*, 1990, 1687.
2 G. Blasse, G. T. Dirkssen and F. Zonnevijile, *J. Inorg. Nucl. Chem.*, 1981, **43**, 2847; *Chem. Phys. Lett.*, 1981, **83**, 449.
3 R. Ballardini, Q. G. Mulazzani, M. Venturi, F. Balletta and V. Balzani, *Inorg. Chem.*, 1984, **23**, 300; R. Ballardini, E. Chiorboli and V. Balzani, *Inorg. Chim. Acta*, 1984, **95**, 323.
4 J. R. Darwent, C. D. Flint and P. J. O'Grady, *Chem. Phys. Lett.*, 1986, **127**, 547.
5 H. Naruke and T. Yamase, *Denki Kagaku*, 1990, **58**, 507; H. Naruke, T. Ozeki and T. Yamase, *Acta Crystallogr.*, 1990, in the press.
6 W. D. Harrocks, jun. and D. R. Sudnick, *Acc. Chem. Res.*, 1981, **14**, 384; V. Balzani, N. Sabbatini and F. Scandala, *Chem. Rev.*, 1986, **86**, 319.
7 Nippon Bunsekikagakukai (ed.), *Bunsekikagaku Binran*, Maruzen, Tokyo, 1961, p. 86.
8 R. D. Peacock and T. J. R. Weakly, *J. Chem. Soc. A*, 1971, 1836.
9 T. Yamase and T. Ikawa, *Bull. Chem. Soc. Jpn.*, 1977, **50**, 746.
10 I. Boschen, B. Buss and B. Krebs, *Acta Crystallogr., Sect. B*, 1974, **30**, 48.
11 S. Ohba, *Manual for CHAGE system*, ed. T. Itoh, Computer Center of Tokyo University, Tokyo, 1986, p. 22.
12 P. Main, S. E. Hull, L. Lessinger, G. Germain, P. J. Declercq and M. M. Woolfson, MULTAN 78, A System of Computer Programs for the Automatic Solution of Crystal Structures from X-Ray, Diffraction Data, University of York, 1978.
13 *International Tables for X-Ray Crystallography*, Kynoch Press, Birmingham, 1974, vol. 4, pp. 99 and 149; D. T. Cromer and D. Liberman, *J. Chem. Phys.*, 1970, **53**, 1891.
14 G. M. Sheldrick, SHELX 76, Program for Crystal Structure Determination, University of Cambridge, 1976.
15 Y. Haas and G. Stein, *J. Phys. Chem.*, 1971, **75**, 3668.
16 C. Rocchiccioli-Deltcheff, R. Thouvenot and M. Fournier, *Inorg. Chem.*, 1982, **21**, 30.
17 C. Rocchiccioli-Deltcheff, M. Fournier, R. Franck and R. Thouvenot, *Inorg. Chem.*, 1983, **22**, 207.
18 H. Kang, S. Liu, S. N. Shaikh, T. Nickolson and J. Zubieta, *Inorg. Chem.*, 1989, **28**, 920.
19 G. Blasse, *Handbook on the Physics and Chemistry of Rare Earths*, vol. 4, eds. K. A. Gschneidner and L. Eyring, North-Holland, Amsterdam, 1979, p. 209; *Struct. Bonding (Berlin)*, 1980, **42**, 1.
20 W. D. Horrocks, jun. and M. Albin, *Prog. Inorg. Chem.*, 1984, **31**, 1.
21 J. Forsberg, *Coord. Chem. Rev.*, 1973, **10**, 195.
22 T. Yamase and R. Watanabe, *J. Chem. Soc., Dalton Trans.*, 1986, 1669.
23 T. Yamase and M. Suga, *J. Chem. Soc., Dalton Trans.*, 1989, 661.
24 T. Yamase and T. Usami, *J. Chem. Soc., Dalton Trans.*, 1988, 183.
25 T. Yamase, *J. Chem. Soc., Dalton Trans.*, 1987, 1597; Y. Sasaki, T. Yamase, Y. Ohashi and Y. Sasada, *Bull. Chem. Soc. Jpn.*, 1987, **60**, 4285.
26 C. Sanchez, J. Livage, J. P. Launay, M. Fournier and Y. Jeannin, *J. Am. Chem. Soc.*, 1982, **104**, 3194.
27 C. Sanchez, J. Livage, J. P. Launay and M. Fournier, *J. Am. Chem. Soc.*, 1983, **105**, 6817.
28 J. Iball, J. N. Low and T. J. R. Weakley, *J. Chem. Soc., Dalton Trans.*, 1974, 2021.
29 G. Blasse and S. Kemmler-Sack, *Ber. Bunsenges. Phys. Chem.*, 1983, **87**, 352.
30 H. G. Brittain and W. A. McAllister, *Spectrochim. Acta, Part A*, 1985, **41**, 1041.

Received 4*th July* 1990; *Paper* 0/030131